Available online at www.sciencedirect.com

ScienceDirect

journal homepage: www.elsevier.com/locate/he

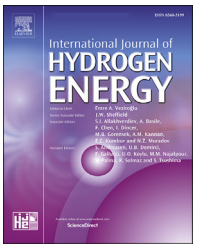

Cold start cycling durability of fuel cell stacks for commercial automotive applications

Tsuyoshi Takahashi [a,b], Yohsuke Kokubo [a], Kazuya Murata [a], Osamu Hotaka [a], Shigeki Hasegawa [a], Yuya Tachikawa [b,c,d], Masamichi Nishihara [c], Junko Matsuda [c,d], Tatsumi Kitahara [b], Stephen M. Lyth [d,e], Akari Hayashi [b,c,d,f], Kazunari Sasaki [b,c,d,f,*]

[a] Commercial ZEV System Products Development Division, Toyota Motor Corporation, Toyota Aichi, 471-8571, Japan
[b] Department of Hydrogen Energy Systems, Faculty of Engineering, Kyushu University, Nishi-ku Fukuoka 819-0395, Japan
[c] International Research Center for Hydrogen Energy, Kyushu University, Nishi-ku Fukuoka 819-0395, Japan
[d] Next-Generation Fuel Cell Research Center (NEXT-FC), Kyushu University, Nishi-ku Fukuoka 819-0395, Japan
[e] Department of Automotive Science, Graduate School of Integrated Frontier Sciences, Kyushu University, Nishi-ku Fukuoka 819-0395, Japan
[f] Platform of Inter-/Transdisciplinary Energy Research (Q-PIT), Kyushu University, Nishi-ku Fukuoka 819-0395, Japan

HIGHLIGHTS

- Cold start cycling tests down to −30 °C on prototype fuel cell stacks were conducted.
- Thinning of the cathode layer up to 13% was observed near the air outlet.
- Ice formation may cause high internal voltage and cathode carbon corrosion.
- Hydrogen crossover easily meets targets under US and Japanese protocols.
- Prototype fuel cell stacks successfully meet the cold start durability targets.

ARTICLE INFO

Article history:
Received 15 June 2022
Received in revised form
13 September 2022
Accepted 17 September 2022
Available online 3 November 2022

Keywords:
Polymer electrolyte fuel cells
Fuel cell electric vehicles

ABSTRACT

System durability is crucial for the successful commercialization of polymer electrolyte fuel cells (PEFCs) in fuel cell electric vehicles (FCEVs). Besides conventional electrochemical cycling durability during long-term operation, the effect of operation in cold climates must also be considered. Ice formation during start up in sub-zero conditions may result in damage to the electrocatalyst layer and the polymer electrolyte membrane (PEM). Here, we conduct accelerated cold start cycling tests on prototype fuel cell stacks intended for incorporation into commercial FCEVs. The effect of this on the stack performance is evaluated, the resulting mechanical damage is investigated, and degradation mechanisms are proposed. Overall, only a small voltage drop is observed after the durability tests, only minor damage occurs in the electrocatalyst layer, and no increase in gas crossover is

* *Corresponding author*. Department of Hydrogen Energy Systems, Faculty of Engineering, Kyushu University, Nishi-ku Fukuoka 819-0395, Japan.
E-mail address: sasaki@mech.kyushu-u.ac.jp (K. Sasaki).

https://doi.org/10.1016/j.ijhydene.2022.09.172

Fuel cell stacks
Cold start cycling durability
Hydrogen crossover
Degradation mechanism

observed. This indicates that these prototype fuel cell stacks successfully meet the cold start durability targets for automotive applications in FCEVs.

Introduction

To contribute to a meaningful decarbonization of society, the automotive industry plans to accelerate the realization of the "connected, autonomous, shared, electric (CASE)" and the "Mobility as a Service (MaaS)" concepts. As such, the electrification of mobility technologies is becoming increasingly important, as already demonstrated in battery electric vehicles (BEVs). More recently, the focus is shifting to fuel cell electric vehicles (FCEVs) as a core technology towards automobile electrification [1–3]. In support of this, the International Energy Agency (IEA) highlighted the importance of fuel cell technologies in its recent "Future of Hydrogen" report [4]. For example, in 2014, Toyota began commercialization of its 1st generation FCEV, the MIRAI, towards the goal of automobile electrification [5–9]. The new Toyota MIRAI model, incorporating the 2nd generation fuel cell stack system was released in December 2020, as shown in Fig. 1: (a) FCEV, (b) FC system, and (c) single cell consisting of an MEA and separators [10–13].

For the popularization of FCEVs as commercial products, sufficient reliability and durability of the fuel cell system are essential, and many reports have discussed durability issues in fuel cell systems [14,15]. Two main factors have been proposed in the deterioration of fuel cell system performance. One is performance drop due to degradation of the electrocatalyst layer [16–19]. Another is increased gas crossover due to degradation of the polymer electrolyte membrane (PEM) [20–24].

Degradation of the electrocatalyst layer is attributed to platinum dissolution (induced by fluctuating cell voltage); Ostwald ripening (due to redeposition on larger Pt nanoparticles); platinum aggregation (due to weak metal-support interaction between Pt-based catalysts and carbon supports), and electrode thinning (due to oxidation and gasification of the carbon support). Meanwhile, degradation of the PEM is attributed to membrane thinning by peroxide radical attack; pinhole and crack formation in the cell due to dry-wet cycling; and/or volumetric changes resulting from ice formation. The relationship between radical generation under open circuit voltage (OCV) conditions and membrane thinning has been previously investigated [25]. For example, Kreitmeier et al. performed qualitative analysis of pinhole formation using Fourier transform infrared spectroscopy (FT-IR) combined with microscopic observation [24].

Durability evaluation of PEMs is generally performed using four different protocols: (i) OCV holding tests to highlight chemical degradation; (ii) wet-dry cycling tests to evaluate mechanical deterioration; (iii) start-stop cycling tests; and (iv) load cycling tests. These protocols have been standardized by the United States Fuel Cell Council (USFCC) and the United States Department of Energy (DOE) [26,27]. Similarly in Japan, the Fuel Cell Commercialization Conference of Japan (FCCJ), the New Energy and Industrial Technology Development Organization (NEDO), and the Japan Automobile Research Institute (JARI) have also proposed their own standardized evaluation protocols [28–30].

In real-world applications, sometimes FCEV systems must be operated in sub-zero conditions, where the water already inside the cell is frozen. However, mechanical damage due to ice formation in cold climates has not yet been included in such standardized evaluation protocols mentioned above. Even in sub-zero conditions, the water generated in a PEFC can remain in a supercooled liquid state for some time after start up [31,32]. If this supercooled state is not maintained, a

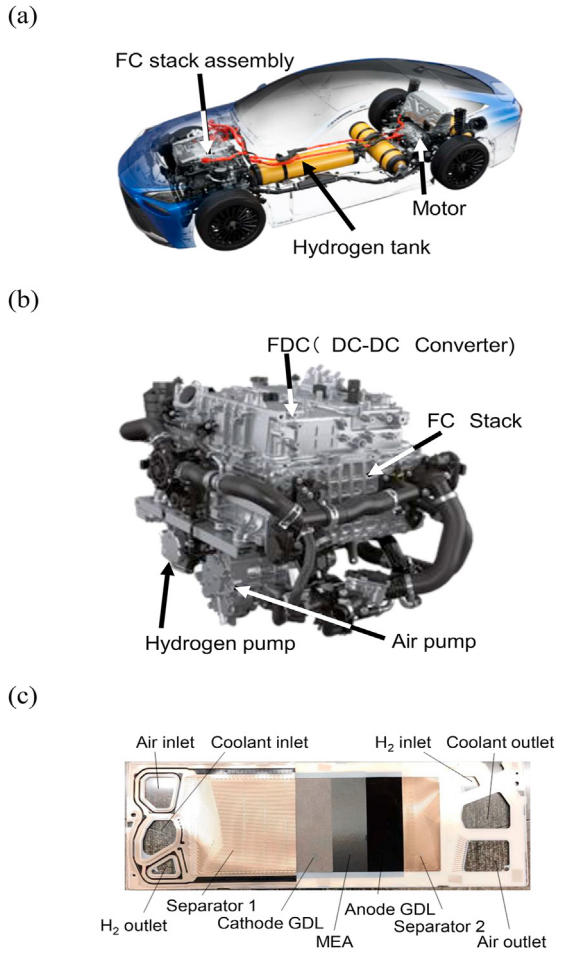

Fig. 1 – (a) Schematic image of the 2nd-Generation Toyota MIRAI FCEV. (b) 2nd-Generation fuel cell stack assembly with balance of plant. (c) Single fuel cell module including a membrane electrode assembly (MEA) and separators.

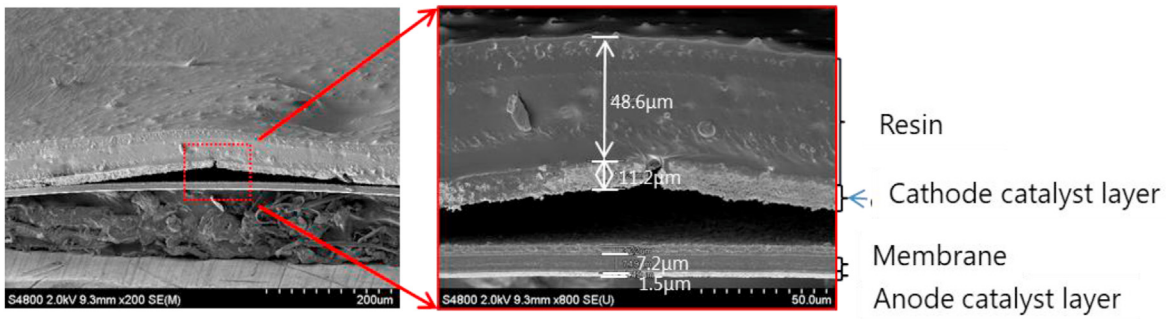

Fig. 2 – Cross-sectional images of typical damaged MEAs observed by FE-SEM.

sudden phase transition to the solid state can occur. The resulting formation of solid ice crystals within the PEFC might cause e.g. delamination of the PEM from the electrocatalyst layer; mechanical damage to the PEM; or cracking of the microporous layer and/or electrocatalyst layer, as shown in Fig. 2. Several investigations into the performance of PEFCs in cold conditions have been published [33,34]. For example, Biesdorf et al. reported a clear dependance on electrode area for the cold start capability of PEFCs, with smaller electrodes resulting in improved performance [33]. Meanwhile, Chikahisa et al. reported visualization of water generated in the electrocatalyst layer in sub-zero conditions using cryo scanning electron microscopy [35], as well as showing the dependance of the mechanical damage on the start-up temperature [36].

In the case of FCEV operation in cold climates, a rapid start-up process can be employed to warm up the fuel cell system before use [31]. A typical polarization curve under normal fuel cell operating conditions is shown in Fig. 3. The red circle corresponds to the point of normal operation, and the area A is proportional to the waste heat generated during operation. Meanwhile, a typical polarization curve measured under rapid start-up conditions is also shown in Fig. 3. Under rapid start-up conditions, the air flow is reduced compared with normal operating conditions to increase the concentration overvoltage and intentionally lower the fuel cell efficiency. In addition, the current density is much higher than under normal operating conditions. Together, these factors result in the generation of excess heat (proportional to the sum of areas A and B). This allows the catalyst layer to heat up, increasing the temperature to above its freezing point (>0 °C), and allowing the fuel cell system to operate normally. During rapid start-up operation in FCEVs, each cell in the prototype fuel cell stack is monitored and controlled to ensure the voltage is always above 0 V.

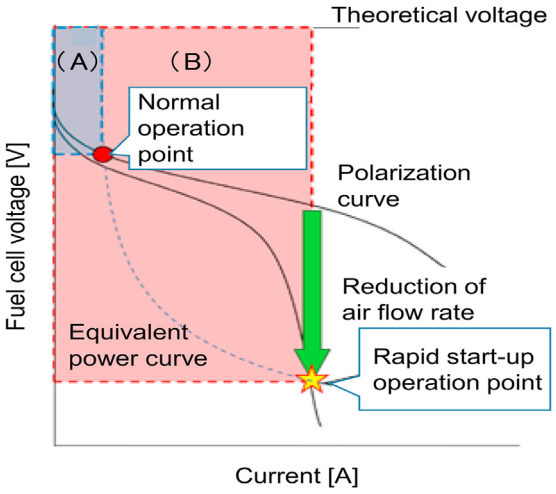

Fig. 3 – Summary of the rapid cold start-up protocol concept. Area (A) is proportional to the heat generated during normal operation. Area (A)+(B) is proportional to the heat generated during rapid cold start-up.

Evaluation of PEFCs and elucidation of the degradation phenomena after cold start operation are of great importance for the mass-production and commercialization of FCEVs. However, to the best of our knowledge, accelerated cold start cycling tests of fuel cell stacks have not yet been reported. As such, here we conduct such tests using in-house protocols on a prototype fuel cell stack designed for integration into a commercial FCEV, and clarify the effect of ice formation within the system via microscopic observation and electrochemical evaluation.

Experimental procedure

Prototype fuel cell stack

The prototype fuel cell stack prepared for this study consisted of 20 single cells in the stacks for cold start cycling durability tests. A single cell module (sectioned to display the different components) is shown in Fig. 1 (c), and this was subjected to accelerated cold start stress tests. This stack was designed and built in-house by Toyota Motor Corporation. Each cell comprised a membrane electrode assembly (MEA) sandwiched between carbon paper gas diffusion layers (GDLs) and metal titanium separators, and was sealed using a proprietary thermoplastic gasket [10,11]. Mesoporous carbon nanodendrite (MCND) supports decorated with Pt–Co alloy catalysts were employed at the cathode [11]. Meanwhile a Pt catalyst decorated on carbon black was used at the anode. The Pt loading was 0.17 mg-Pt cm^{-2} at the cathode, and 0.025 mg-Pt cm^{-2} at the anode. An ionomer with three times higher oxygen permeability compared to conventional Nafion ionomers was used in the electrocatalyst layers [37]. Separator 1 uses a "partially straight flow field", and both separators are

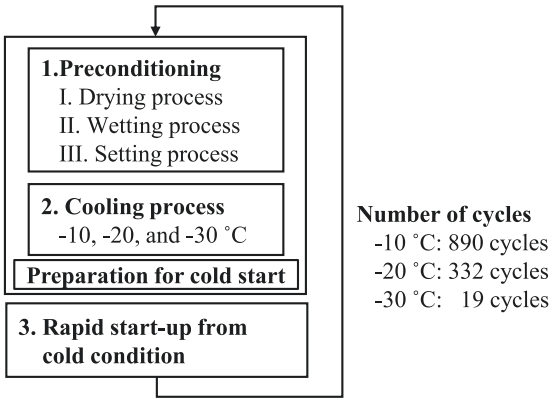

Fig. 4 – Cold start cycling test protocol. The starting temperature for each cycle is either −10, −20, or −30 °C. The selected number of cycles at each temperature was determined based on typical climate information in Canada.

coated with a titanium oxide (TiO_x) and carbon nanocomposite layer to improve electronic conductivity and minimize contact resistance [10–13]. The hydrogen and air gas inlets were both located at the positive terminal side of the stack, and separately supplied to the anode and cathode via a flow field. Coolant (water mixed with ethylene glycol) was introduced through a separate flow field system.

Rapid start-up cycling tests in sub-zero conditions

Rapid start-up cycling tests of fuel cell stacks under cold conditions included three main steps: (i) preconditioning; (ii) cooling; and (iii) rapid start-up, as shown in Fig. 4. Detailed experimental conditions are compiled in Table 1. Typical data of one cycle with these three steps is shown in Fig. 5. Three different temperatures and the number of cycles were selected according to temperature and climate data obtained in Quebec, Canada from 2010 to 2012 [38]. In this study, this translates to 890 cycles at −10 °C; 332 cycles at −20 °C; and 19 cycles at −30 °C, or a total of 1241 cycles, equivalent to an FCEV lifetime of 15 years in Canada. The order of measurement of the different temperatures was −20 °C, −10 °C, and then −30 °C. Rapid start-up from the extreme temperature of −30 °C is rarely required in the real world, and therefore cycling at this temperature was performed at the end.

Within the preconditioning step, three separate sub-steps were employed to ensure a constant amount of water in the stack throughout the cold start cycling test. The specific conditions of each step are summarized in Table 1. First, a drying process was applied to the fuel cell stack using relatively high gas flow rates, until a cell resistance exceeds 5 Ω cm^2 at 25 °C (monitored via cell impedance). Second, a wetting procedure was applied by operating the fuel cell stack system at a constant current density of 0.2 A cm^{-2}, until the stack temperature increased from 25 to 62 °C (monitored via the temperature of the coolant fluid). Thirdly, 80% of water (relative to the fully humidified condition) was removed from the fuel cell stack in a setting step, by flowing dry air through the system for 40 s (decreasing the stack temperature from 62 to 58 °C). After the preconditioning step, the stack was subjected to a cooling step. In this step, the system was cooled to either −10, −20, or −30 °C for 50 min, by placing the fuel cell stack in a cold chamber and controlling the coolant temperature. Coolant was circulated in the system at all times, maintained at the target temperature by passing it through a recirculating chiller with sufficient cooling capability. The thickness of the Ti foil separators was only ~100 μm, so that the cell temperature can be assumed to be the same as the coolant temperature. Before starting each measurement, it was verified that the coolant temperature was at the target temperature. Finally, the rapid cold start step was performed, until the coolant temperature increased from the starting temperature up to 30 °C.

To warm up the fuel cell system using the rapid start-up procedure shown in Fig. 3 [31], power generation was initiated (at 5220 s in Fig. 5) and maintained at 0.75 A cm^{-2} by controlling the cell voltage at around 0.1 V. Detailed evaluation conditions are compiled in Table 2. The coolant temperature increased and reached 0 °C at the outlet after 140 s (at 5360 s in Fig. 5). The current density was then changed to 1.0 A cm^{-2}, and the coolant temperature further increased, reaching 30 °C after 480 s (at 5700 s in Fig. 5).

Table 1 – Summary of the three different steps during the preconditioning procedure.

Procedure		Drying	Wetting	Setting
Coolant temp. [°C]		70 → 25	25 → 62	62 → 58
Current density [A cm^{-2}]		–	0.2	–
Gas flow rate	Flow rate [L min^{-1} $cell^{-1}$]			
	Anode	3.5	–	0.56
	Cathode	10	–	3.6
	Stoichiometric ratio			
	Anode	–	2.2	–
	Cathode	–	1.8	–
Gas temp. [°C]	Anode	80	80	25
	Cathode	80	80	25
Gas dew point [°C]	Anode	–	45	−40
	Cathode	–	−40	−40
Gas pressure [kPa abs.]	Anode	–	160	160
	Cathode	–	100	100
Time period		Until cell impedance exceeds 5 Ω cm^2.	Until coolant temperature reaches 62 °C.	40 s.

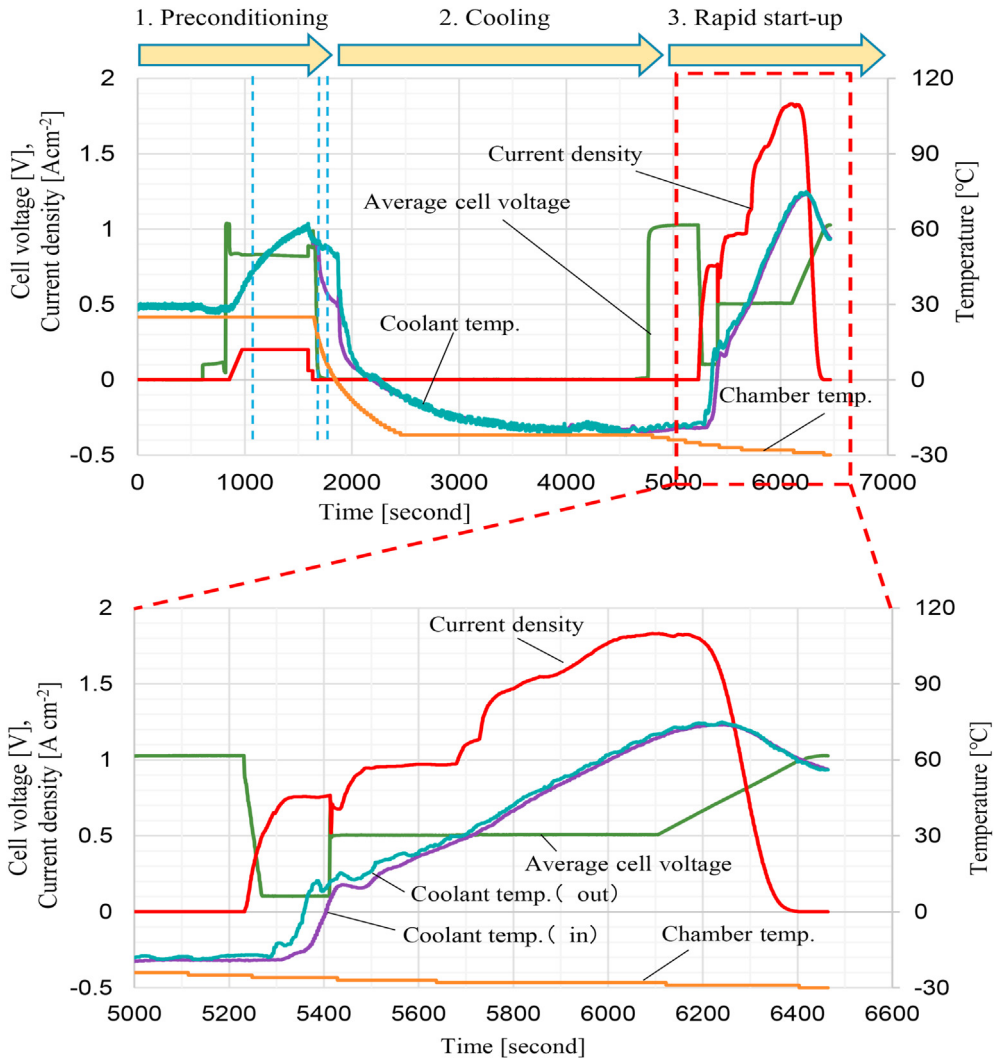

Fig. 5 – Typical data obtained from one cycle test consisting of three steps (preconditioning, cooling, and rapid start-up), from low temperature (the case of −20 °C).

Hydrogen crossover leak tests

Quantification of damage in the fuel cell stack was carried out by electrochemical gas crossover leak tests at each individual cell. The hydrogen crossover across the cells in the stack was measured *in-situ* without disassembling the stack, using the following procedures.

First, the anode side of the cell stack was filled with hydrogen gas under static conditions, and nitrogen gas was supplied to the cathode at 1.0 L min^{-1} and 40 °C. The voltage due to hydrogen permeation through the polymer electrolyte membrane from the anode to the cathode was measured, and the hydrogen crossover was calculated from the Nernst equation:

$$E = 2.3026 \times (RT/2F) \times \log_{10} [P_{H2(a)}/P_{H2(c)}] \quad (1)$$

$$P_{H2(c)} = P \times \varphi_{H2} / Z_{N2} \quad (2)$$

where E is the cell voltage (V); $P_{H2(a)}$ is the hydrogen pressure (kPa absolute) at the anode; and $P_{H2(c)}$ is the hydrogen pressure at the cathode. R is the gas constant (8.31 J mol^{-1} K^{-1}); T is the temperature (K); and F is the Faraday constant (96,500 C mol^{-1}). P is the nitrogen pressure (kPa absolute) at the cathode; Z_{N2} is the flow rate of N_2 gas at the cathode; and φ_{H2} is the rate of hydrogen crossover.

Evaluation of in-plane current distribution in the fuel cell stack

To confirm the degradation mechanism precisely, the current distribution of the fuel cell stack was measured. This current distribution measurement was made using a stack with 13 cells, rather than 20 cells for the cold start cycling durability tests. Fig. 6 shows the plate-like current detector with segmented terminals. Experimental conditions for the current distribution measurements are compiled in Table 2. This detector, shown in Fig. 6 with 59 segmented terminals, was inserted between the 6th cell and the 7th cell at the middle of the 13-cell stack. Current density distribution was evaluated from current density values detected at each terminal. The resistance of the gold-based terminals was considered low enough for accurate current density measurements.

Table 2 – Experimental conditions during the "setting" preconditioning step and the cold start step.

Process		Setting	Cold start
Coolant	Temp. [°C]	62	–
	Flow rate [L min^{-1} $cell^{-1}$]	0.5	–
Current density [A cm^{-2}]		0.06	0–1.2
Gas flow rate	Flow rate [L min^{-1} $cell^{-1}$]		
	Anode	0.56	–
	Cathode	3.6	–
	Stoichiometric ratio		
	Anode	–	1.3
	Cathode	–	<1.0
Gas temp. [°C]	Anode	–	80
	Cathode	–	80
Gas dew point [°C]	Anode	45	–
	Cathode	−40	–
Gas pressure [kPa abs.]	Anode	160	240
	Cathode	100	140
Time period		180 s.	Until coolant temperature reaches 30 °C

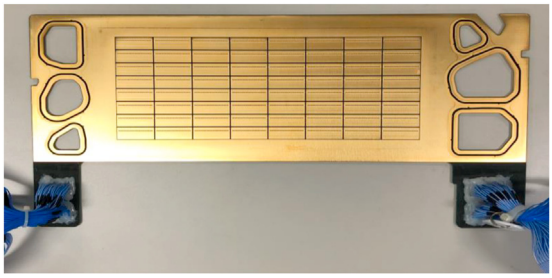

Fig. 6 – Segmented terminals for current distribution analysis.

Cyclic voltammograms

Cyclic voltammetry (CV) was conducted to confirm electrochemical surface area (ECSA) before and after the cold start cycling test. Before CV measurements, a pretreatment step was applied to stabilize the measurement conditions, in which hydrogen gas was supplied to the anode at 2 L min^{-1} and 200 kPa absolute pressure, and nitrogen gas was supplied to the cathode at 4 L min^{-1} and 100 kPa absolute (i.e., atmospheric pressure). The dew point of both gases was 50 °C. After this pretreatment step, the hydrogen and nitrogen supplies were interrupted, and CV measurements were conducted in the closed environment at 30 °C (200 kPa absolute pressure of hydrogen on the anode side, and 100 kPa absolute pressure of nitrogen on the cathode side). The voltage measurement range was between 0.05 and 1.0 V, and the scan rate was 50 mV s^{-1}. The voltage was cycled 5 times, and average spectra were obtained from the 2nd to 5th cycles.

SEM observation of the cross sections of the electrocatalyst layer

The microstructure of the electrocatalyst layers after cold start cycling tests was observed by scanning electron microscopy (SEM, S-4800, Hitachi High-Technologies, Japan) with an acceleration voltage of 2.0 kV. Secondary electron images were recorded.

Results and discussion

Stack performance

Using a stack with 20-cells, the average voltage per cell measured at 2.2 A cm^{-2} throughout the cold start cycling test is shown in Fig. 7 (a). The average voltage drops per cycle at −10, −20, and −30 °C were 12, 18, and 316 μV $cycle^{-1}$,

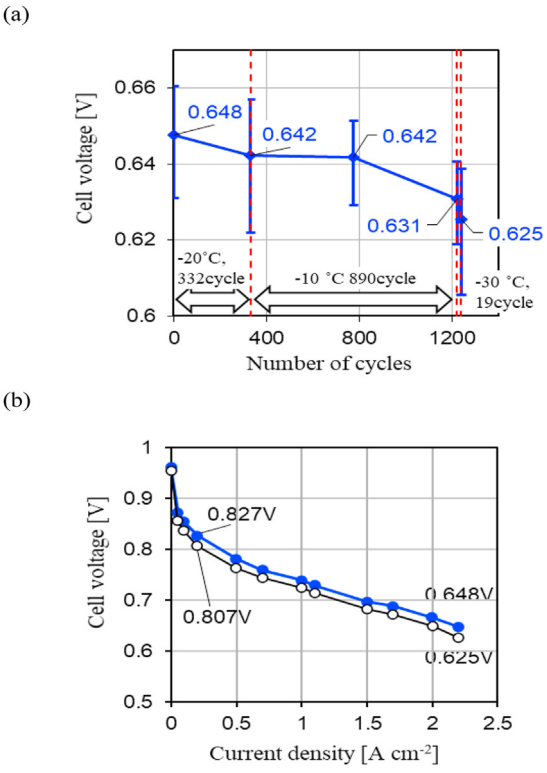

Fig. 7 – (a) Plot of the average cell voltage during the cold start cycling test, obtained at 2.2 A cm^{-2}. (b) Current-voltage curves before (filled circles) and after (open circles) the cold start cycling test.

respectively. This gives an indication of the effect of supercooled water generated in the cell [31,32]. If the temperature is higher than −20 °C, the heat generated during the rapid start-up process (Fig. 3) works effectively to maintain the (liquid) water in a supercooled state until the temperature increases to >0 °C, resulting in a relatively small voltage drop. In contrast, at −30 °C, it is likely that some of the generated water freezes immediately, causing physical damage and resulting in a larger voltage drop.

The current-voltage performance of the stack was measured before and after the cold start cycling test, as shown in Fig. 7 (b). At a relatively low current density of 0.2 A cm^{-2} (i.e. 12 % of the maximum power density, corresponding to averaged FCEV usage), the initial cell voltage was 0.827 V, slightly dropping to 0.807 V after the cold start cycling test. This represents a voltage drop of just 20 mV, or 2.4%. At the relatively high current density of 2.2 A cm^{-2} (corresponding to the maximum power density of the stack), the initial cell voltage was 0.648 V, dropping to 0.625 V after the cold start cycling test. This represents a voltage drop of only 23 mV, or 3.5%. In both cases, these voltage drops easily meet our tentative in-house durability target for cold start operation of an FCEV, namely a performance drop of less than 5% over 15 years. The durability up to 1241 cycles successfully demonstrated in this study provides evidence of sufficient water management, whereas inhomogeneous water distribution would lead to mechanical damage due to ice formation. These results indicate that the rapid start-up process can be applied effectively in FCEVs in cold regions without sacrificing durability, although the performance drop is more significant under harsher conditions, i.e. at −30 °C and below.

Gas crossover

Hydrogen crossover is a key indicator in the assessment of PEM degradation by mechanisms such as membrane thinning and pinhole formation. During the cold start process, physical damage to the PEM by ice formation should be considered. Hydrogen crossover values should be quantified and compared with the targets specified by various organizations. As such, hydrogen crossover was measured for each cell in the stack during the cold start cycling test, as shown in Fig. 8. The degree of hydrogen crossover did not change throughout the test, clearly demonstrating that physical degradation of the PEM via ice formation is not induced under cold start operation. Moreover, the value obtained for hydrogen crossover, namely 15 nmol s^{-1} cm^{-2}, is well within our tentative in-house criteria (target) of 30 nmol s^{-1} cm^{-2}. Here, it should be noted that hydrogen crossover measured in this study is defined in units of nmol s^{-1} cm^{-2}. Meanwhile, hydrogen crossover targets specified by the DOE and the USFCC are stated in mA cm^{-2}. These two different unit systems are related to each other through the following equation:

$$\text{Hydrogen crossover current density [mA cm}^{-2}\text{]} = \text{Hydrogen crossover [nmol s}^{-1}\text{ cm}^{-2}\text{]} \times F\ [\text{A s mol}^{-1}\ (\text{C mol}^{-1})] \times n \times 10^{-6} \quad (3)$$

where F is the Faraday constant, and n is the number of electrons in the hydrogen molecule (i.e., 2). The target of

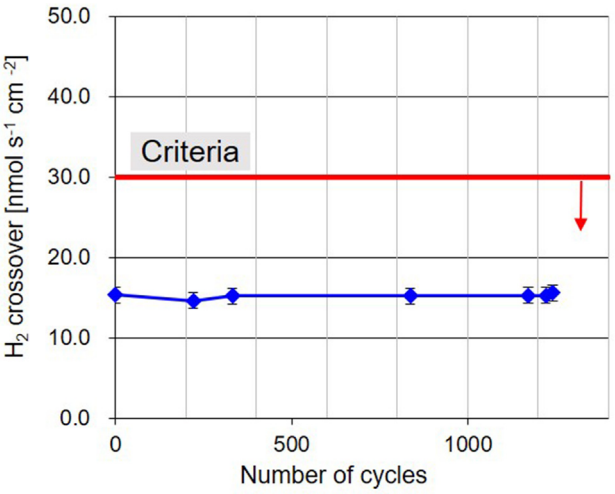

Fig. 8 – Hydrogen crossover during the cycle test (blue). Average, maximum, and minimum values are shown. Tentative criteria (target) of hydrogen crossover for FCEVs (red) are also shown. (For interpretation of the references to color/colour in this figure legend, the reader is referred to the Web version of this article.)

Table 3 – Targets of hydrogen crossover and hydrogen crossover current density, specified in DOE, USFCC [26], and FCCJ [27–29] protocols. In-house targets are also shown.

Sources	Target values	
	Hydrogen crossover [nmol s^{-1} cm^{-2}]	Hydrogen crossover current density [mA cm^{-2}]
DOE & USFCC target	103	20
FCCJ target	36–88	7–17
In-house target	30	5.8

hydrogen crossover current density by DOE and USFCC is 20 mA cm^{-2}, which corresponds to hydrogen crossover of 103 nmol s^{-1} cm^{-2} (Table 3), which is significantly higher than our in-house target of 30 nmol s^{-1} cm^{-2}. Meanwhile, the FCCJ sets its hydrogen crossover target as a "10 times increase in hydrogen crossover, compared to the initial value", and defines a suitable hydrogen crossover current density target of

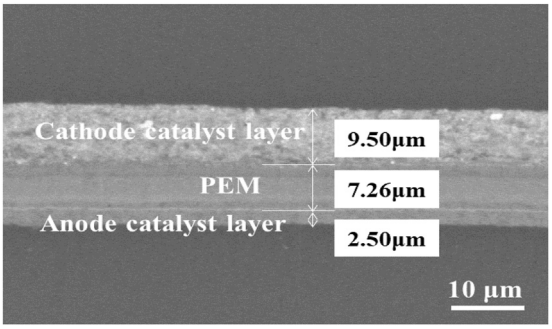

Fig. 9 – Cross-sectional image of the MEA after the cold start cycling test.

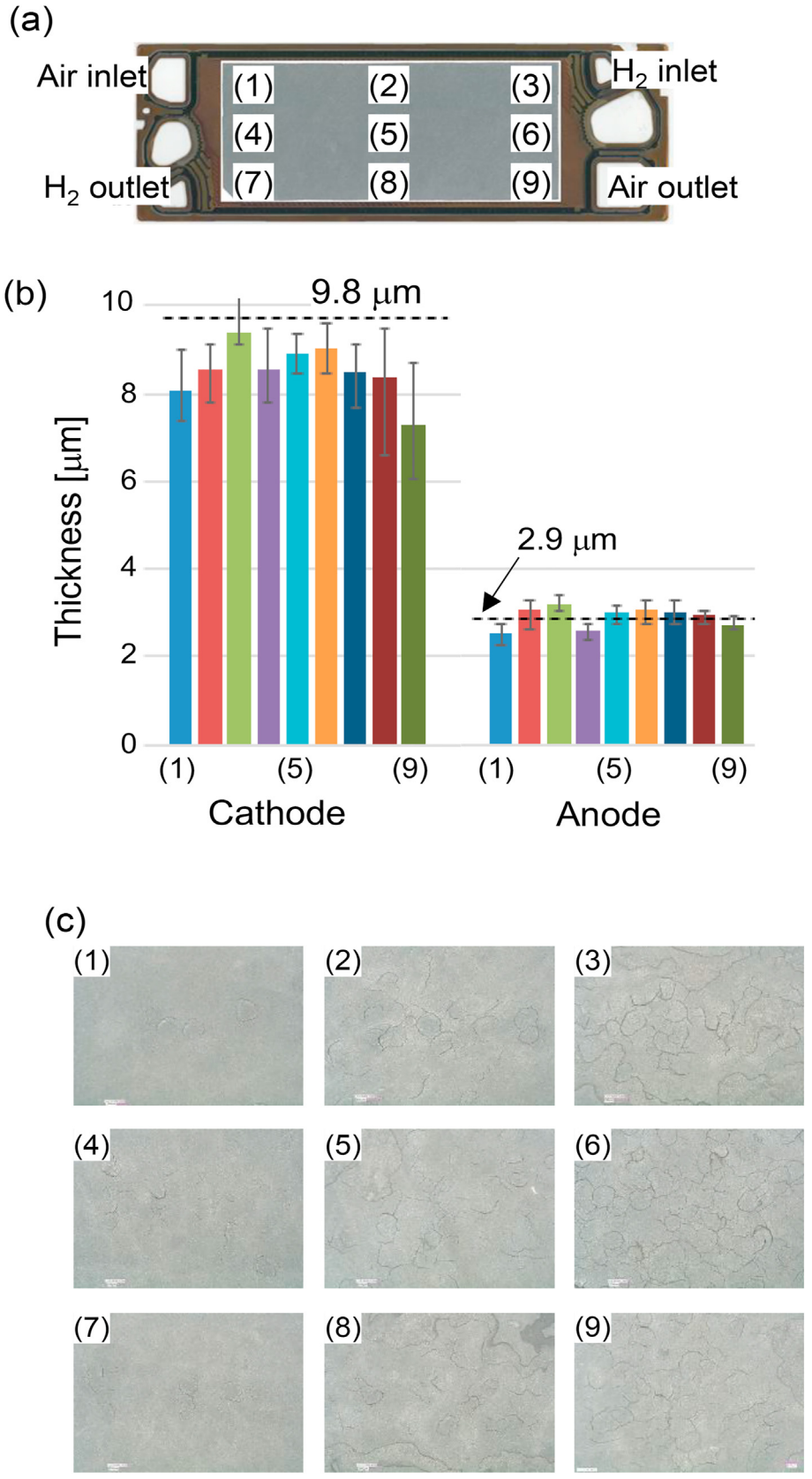

Fig. 10 – (a) Positions of the different measurement positions in the MEAs. (b) Summary of the thickness of the electrocatalyst layers at different positions in the MEA after cycling tests (the dashed line is the thickness before the test). (c) SEM images of the cathode surface of the MEAs at different positions in the MEA, after the cycling test.

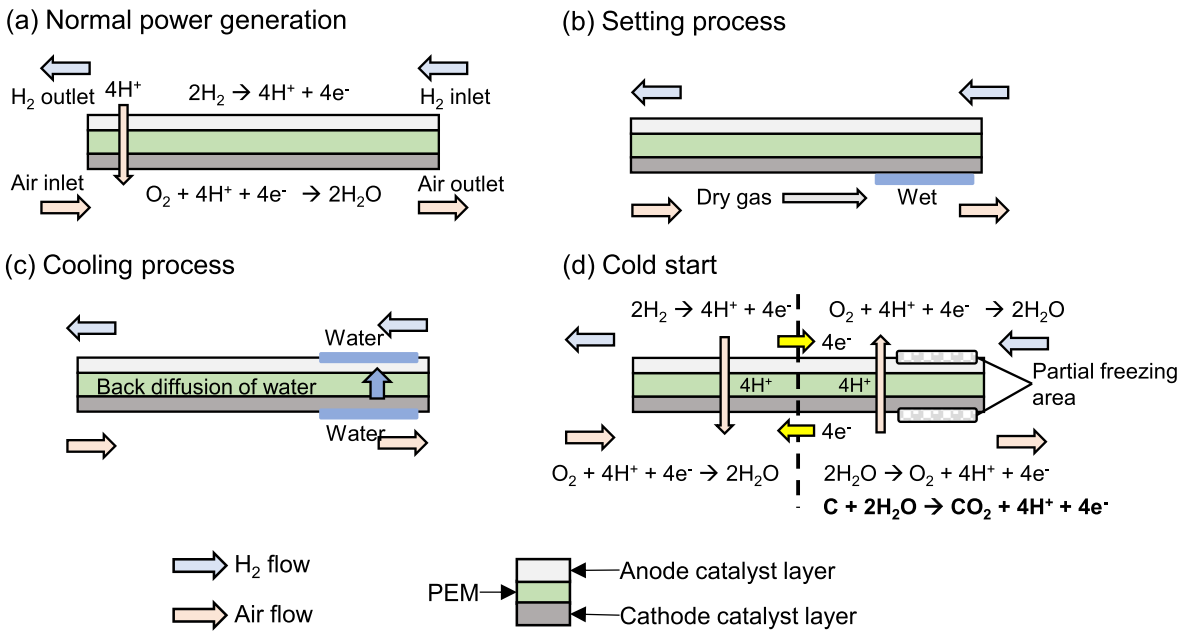

Fig. 11 – Proposed degradation mechanism of the MEA during cold start cycling. (a) Normal operation conditions. (b) Situation during the setting process (see Table 1), in which the dry conditions are induced near the air inlet, but humid (wet) conditions remain near the air outlet. (c) Situation during the cooling process, in which water back diffuses from the cathode to the anode. (d) Situation during cold start operation, in which the internal voltage in the cathode results in carbon corrosion.

around 7–17 mA cm^{-2}. These values correspond to hydrogen crossover of 36–88 nmol s^{-1} cm^{-2}, which again is much higher than our in-house target (Table 3). As such, the hydrogen crossover values obtained in this study meet the US DOE and USFCC target [26], the FCCJ target [27–29], as well as our in-house target, confirming sufficient durability of the PEM against cold start operation.

Microstructural observation

To confirm if any physical damage occurred in the fuel cell stack after cold start cycling tests, microstructural evaluation was carried out on the MEAs by SEM observation. In cross-sectional SEM images, no delamination is observed between the catalyst layer and the PEM, as shown in Fig. 9. This confirms that the MEAs are relatively tolerant to ice formation during the cold start cycling tests.

Thickness evaluation of the electrocatalyst layer was performed via cross-sectional observation at 9 different locations within the MEA shown in Fig. 10 (a). The average initial thickness of the anode electrocatalyst layer before the cold start cycling tests was 2.9 μm, as shown with the dashed line in Fig. 10 (b). After the test, the average thickness did not significantly change, indicating that the rapid cold start process does not affect the anode electrocatalyst layer. No significant variation in anode thickness was observed depending on the location within the MEA.

In contrast, the average initial thickness of the cathode electrocatalyst layer was 9.8 μm, as also shown with the dashed line in Fig. 10 (b). After the cold start cycling test, this decreased to 8.5 μm in average, corresponding to a reduction in thickness of ~13%. In addition, a certain variation in the cathode thickness was observed depending on the location within the MEA. Near the air outlet (i.e., position No. 9 in Fig. 10 (a)), thinning of the cathode electrocatalyst layer was more significant than at any other location, and this is likely to be attributed to carbon gasification. SEM observation of the surface of the cathode electrocatalyst layer was also performed at 9 different locations within the MEA, as shown in Fig. 10 (c). A similar variation with position was observed, with very few cracks observed in the electrocatalyst layer near the air inlet (positions No. 1, 4 and 7), but more cracking in the middle of the MEA (positions No. 2, 3, 5, 6, and 8), and the largest degree of cracking in the electrocatalyst layer near the air outlet (position No. 9), shown in Fig. 10 (c). This cracking in the electrocatalyst layer is attributed to repeated expansion and contraction during the cycling test, resulting in mechanical stresses. The mechanisms for increased degradation in the cathode compared to the anode, and the increased degradation in the region of the air outlet will be discussed in more detail in the next section.

Degradation mechanisms

According to the literature, a major mechanism for MEA degradation during start up is a reduced hydrogen concentration at the anode, resulting in a local increase in voltage at the cathode, in turn causing carbon support oxidation [39,40]. Under cold start up conditions, it is probable that the generation of high voltage and subsequent carbon support oxidation in the cathode is due to a disruption of the hydrogen supply at the anode resulting from ice formation.

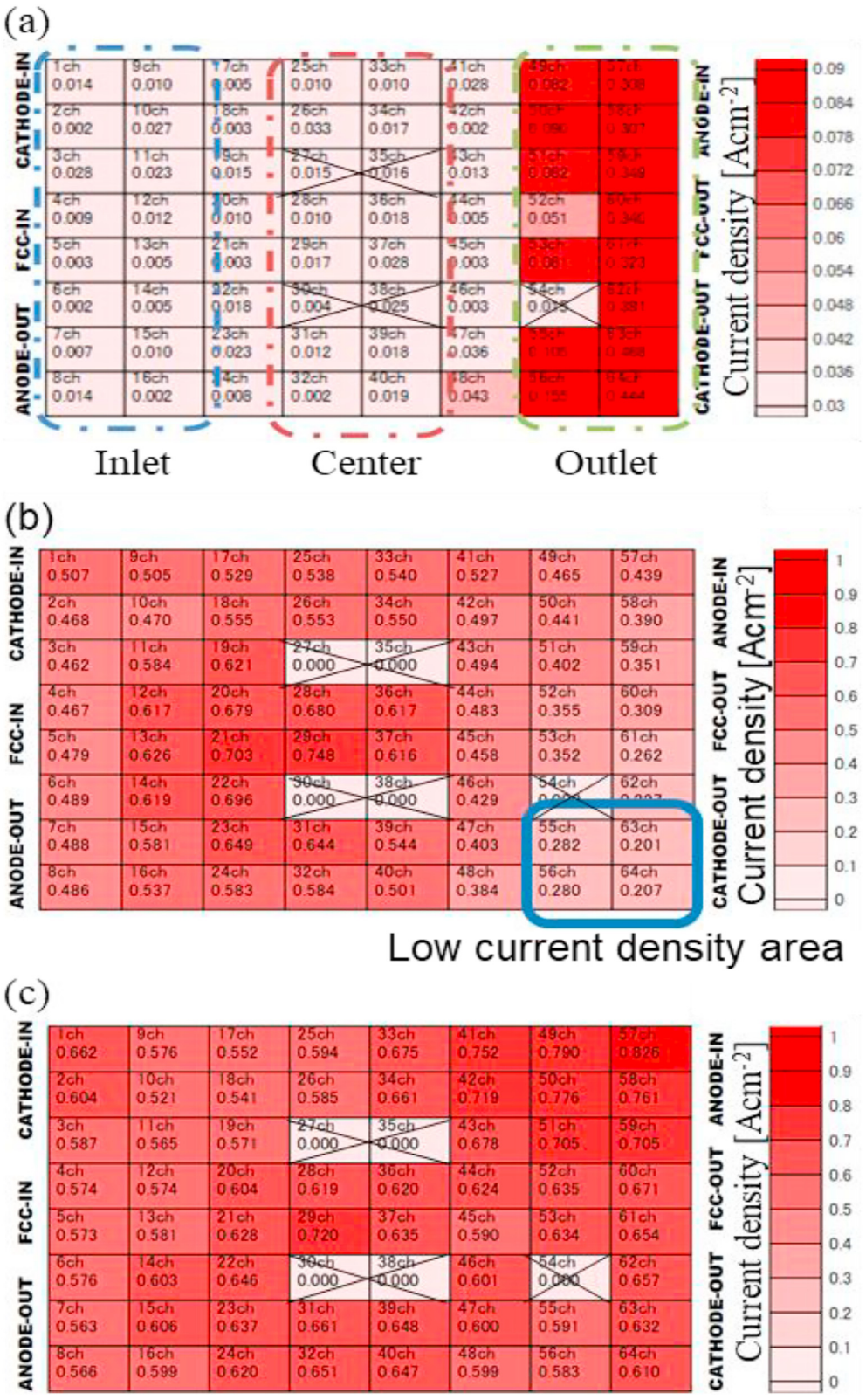

Fig. 12 – Summary of the current density distribution within the MEAs. (a) Drying process, cold start at (b) 0 and (c) 70 s.

This phenomenon is schematically explained in Fig. 11. During normal power generation, water is generated at the cathode (Fig. 11 (a)). During the setting process in the preconditioning step, some of the generated water remains near the region of the air outlet (Fig. 11 (b)). During the cooling step, some of the remaining water molecules diffuse through the thin electrolyte membrane to the anode side of the MEA (Fig. 11 (c)). The remaining water at the anode and cathode then

freezes, and the generated ice layer locally disrupts the hydrogen supply at the anode (Fig. 11 (d)). At the corresponding region in the cathode, the remaining liquid water undergoes the oxygen evolution reaction, generating oxygen gas molecules, protons, and electrons. This creates a high internal voltage within the cathode, especially near the air outlet where the concentration of water is higher, leading to carbon oxidation, and eventually resulting in thinning of the cathode electrocatalyst layer. This is a similar phenomenon to the well-known carbon corrosion up to 1.5 V during conventional start-up of FCEVs [39,40].

To confirm this proposed degradation mechanism, the current distribution across the surface of the MEA was evaluated during the setting stage of the preconditioning step, and during the cold start step (Table 1), using the current distribution analysis system (Fig. 6). In this experiment, the measurement conditions were slightly modified from the cold start cycling test conditions, summarized in Table 2. As shown in Fig. 12 (a), these measurements confirm that the current density is higher near the air outlet during the setting stage, due to the higher concentration of water in this region. The inlet region is relatively dry compared with the outlet region, because dry air was supplied to remove excess water during the excess water removal procedure. In case of the cold start, the excess water in the fuel cell stack would result in mechanical damages shown in Fig. 2.

From the proposed degradation mechanism, it is expected that ice formed near the outlet hinders proper power generation in this region. In fact, at the beginning of the cold start step (i.e. at 0 s), as shown in Fig. 12 (b), the current density at the outlet region was lower than that in the other regions, attributed to disrupted hydrogen supply due to ice formation. After 70 s, as shown in Fig. 12 (c), the current distribution is almost equal across all the regions of the MEA, attributed to the fact that ice is no longer present in the cell at this point. Therefore, sufficient attention should be given to the excess water removal procedure in FCEVs when considering cold start operation.

Overvoltage separation

Separation of the different overvoltages before and after the cold start cycling tests (Fig. 7 (b)) revealed no remarkable increase in either the ohmic losses or the concentration overvoltage. This indicates that the activation overvoltage is likely the major factor contributing to the performance drop of the MEA during cold start. To confirm this, the increase in activation overvoltage during the cold start cycling test was determined from the Tafel plot to be 19 mV, as shown in Fig. 13 (a). This value is close to the total voltage drop obtained from the IV curves before and after the cold start cycling tests, i.e., 20 mV at 0.2 A cm^{-2} and 23 mV at 2.2 A cm^{-2}, shown in Fig. 7 (b). This confirms that the increase in activation overvoltage is largely responsible for the decrease in performance during cold start cycling.

Electrochemical surface area (ECSA)

CV measurements were conducted to investigate any changes in the ECSA during the cold start cycling test. The results are

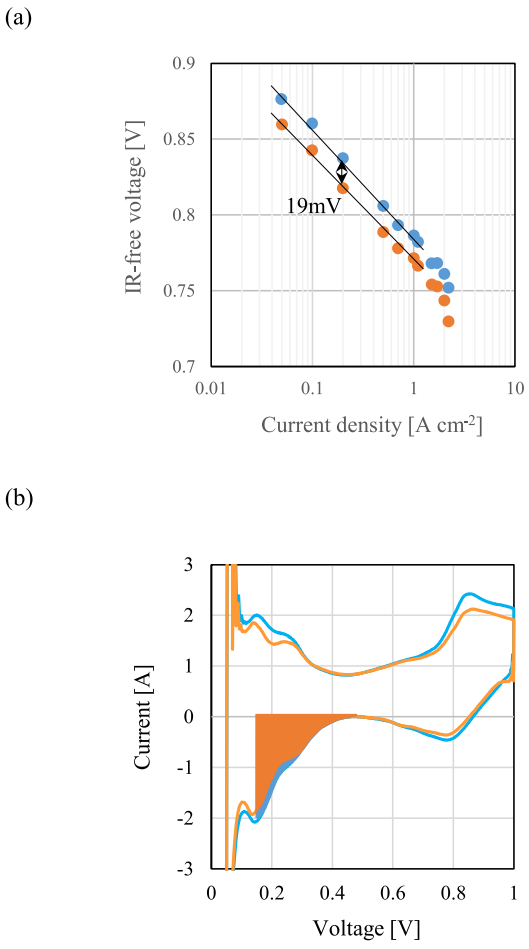

Fig. 13 – (a) IR-free voltage and (b) CV results before (blue) and after (orange) the cold start cycling test. (For interpretation of the references to color/colour in this figure legend, the reader is referred to the Web version of this article.)

shown in Fig. 13 (b). Before the cycling test, the ECSA was 52.2 m^2 g_{Pt}^{-1}, and this dropped to 45.2 m^2 g_{Pt}^{-1} after the test, corresponding to an ECSA retention of 86%. As mentioned previously, the repeated cold-start processes cause damage to the cathode catalyst layers. This damage is especially associated with carbon support corrosion, leading to a decrease in ECSA (as described in Fig. 11) in addition to the typical degradation mechanisms in normal and cold operation as described in the introduction section. According to our in-house database, there is an approximately linear correlation between retention of ECSA and retention of cell voltage after durability tests [41], within the measurement range of CV, as shown in Fig. 14. According to this empirical linear relationship, the ECSA retention of 86% measured here corresponds to a cell voltage retention of 98.3%. As such, the estimated cell voltage after the cold start cycling test is 813 mV, relative to a cell voltage of 827 mV at 0.2 A cm^{-2} before the cycling test. This empirical prediction is very close to the experimentally determined value of 807 mV at 0.2 A cm^{-2} in Fig. 7 (b). These results confirm sufficient durability of the cell stacks against cold start cycling.

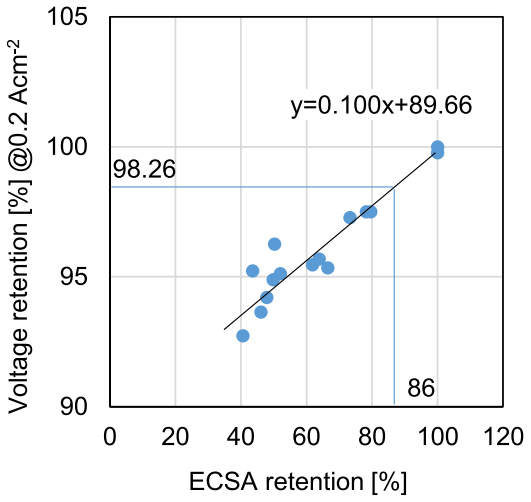

Fig. 14 – Relationship between the retention of ECSA and retention of cell voltage at 0.2 Acm^{-2}.

Conclusions

Cold start cycling tests were carried out on fuel cell stacks to simulate the harsh conditions experienced by FCEVs in cold regions, and the effect of these tests on the catalyst layer and the PEM were evaluated. The cold start cycling test was developed taking into account real-world climatic conditions. The resulting degradation can be assumed to be similar to that experienced by commercial FCEVs.

The performance drop after the cold start cycling test was just 3.5%, meeting our in-house durability target of <5%. Thinning of the cathode electrocatalyst layer was observed, especially near the air outlet. This was attributed to disruption of the hydrogen supply due to ice formation in the anode, resulting in the generation of high internal voltage, and subsequent carbon support corrosion at the cathode. This was confirmed by an observed drop in ECSA, an increase in activation overvoltage, and by current distribution measurements before and after cold start cycling tests. In contrast, gas crossover did not increase during the test, indicating that obvious degradation of the PEM did not occur.

In addition to the mechanistic insights obtained from start-stop cycling tests, load cycling tests, and other reliability tests for fuel cell stacks [5–13,41], the findings of this study have been applied successfully to the development of new fuel cell systems for FCEVs, in particular, the 2nd generation Toyota MIRAI, after carefully comparing 20-cell stacks and 330-cell stacks including the optimization of water management. The results obtained have been applied in the design and development of new FCEV components and systems.

Declaration of competing interest

The authors declare that they have no known competing financial interests or personal relationships that could have appeared to influence the work reported in this paper.

REFERENCES

[1] International Energy Agency. Energy technology perspectives 2017 - Catalysing Energy technology Transformations. 2017. https://www.iea.org/reports/energy-technology-perspectives-2017. [Accessed 24 April 2022].
[2] Hydrogen Council. Hydrogen Scaling up. 2017. https://hydrogencouncil.com/wp-content/uploads/2017/11/Hydrogen-Scaling-up_Hydrogen-Council_2017.compressed.pdf. [Accessed 24 April 2022].
[3] Sasaki K, Li H-W, Hayashi A, Yamabe J, Ogura T, Lyth SM. Hydrogen Energy Engineering: A Japanese perspective. Japan: Springer; 2016.
[4] International Energy Agency. The Future of Hydrogen: Seizing today's opportunities. 2019. https://www.iea.org/hydrogen2019/. [Accessed 24 April 2022].
[5] Kizaki M, Asai H, Yumiya H. Advancing into the future with the Mirai fuel cell system. Toyota Technical Review 2015;61:11.
[6] Hasegawa T, Imanishi H, Nada M, Ikogi Y. Development of the fuel cell system in the Mirai FCV. SAE Tech Pap 2016;1:1185. https://doi.org/10.4271/2016-01-1185.
[7] Maruo T, Toida M, Ogawa T, Ishikawa Y, Imanishi H, Mitsuhiro N, et al. Development of fuel cell system control for sub-zero ambient conditions. SAE Tech Pap 2017;1:1189. https://doi.org/10.4271/2017-01-1189.
[8] Yamashita A, Kondo M, Goto S, Ogami N. Development of high-pressure hydrogen Storage system for Toyota "Mirai. SAE Tech Pap 2015;1:1169–77. https://doi.org/10.4271/2021-01-0741.
[9] Konno N, Mizuno S, Nakaji H, Ishikawa Y. Development of compact and high-performance fuel cell stack. SAE Int J Altern Powertrains 2015;4:123. https://doi.org/10.4271/2015-01-1175.
[10] Takahashi T, Kakeno K, Ikogi K, Imanishi H. Outline of the new fuel cell system in the Second-generation Mirai - development of a fuel cell suitable for mass production -. Toyota Technical Review 2021;66:12.
[11] Mizuno S, Hayashi T, Kubo H, Okumura M, Kurihara T, Mori K. Development of the fuel cell stack for the Second-generation Mirai. Toyota Technical Review 2021;66:22.
[12] Takahashi T. FC system of new MIRAI. Spec Steel 2021;70:11.
[13] Takahashi T. Development of FC system for new MIRAI. J Hydrog Energy Syst Soc Japan 2021;46:135.
[14] Gittleman CS, Kongkanand A, Masten D, Gu W. Materials research and development focus areas for low cost automotive proton-exchange membrane fuel cells. Curr Opin Electrochem 2019;18:81–9. https://doi.org/10.1016/j.coelec.2019.10.009.
[15] Borup RL, Kusoglu A, Neyerlin KC, Mukundan R, Ahluwalia RK, Cullen DA, et al. Recent developments in catalyst-related PEM fuel cell durability. Curr Opin Electrochem 2020;21:192–200. https://doi.org/10.1016/j.coelec.2020.02.007.
[16] Baroody HA, Kjeang E. Predicting platinum dissolution and performance degradation under drive cycle operation of polymer electrolyte fuel cells. J Electrochem Soc 2021;168:044524. https://doi.org/10.1149/1945-7111/abf5aa.
[17] Ramaswamy N, Kumaraguru S, Gu W, Kukreja RS, Yu K, Groom D, et al. High-current density durability of Pt/C and PtCo/C catalysts at similar Particle Sizes in PEMFCs. J Electrochem Soc 2021;168:024519. https://doi.org/10.1149/1945-7111/abe5ea.
[18] Ahluwalia RK, Wang X, Peng J-K, Konduru V, Arisetty S, Ramaswamy N, et al. Achieving 5,000-h and 8,000-h low-PGM electrode durability on automotive drive cycles. J

Electrochem Soc 2021;168:044518. https://doi.org/10.1149/1945-7111/abf507.
[19] Lyth SM, Mufundirwa A. Electrocatalysts in polymer electrolyte membrane fuel cells, Heterogeneous catalysts: Emerging techniques for design, characterization and applications. Wiley-VCH; 2021.
[20] Singh Y, Orfino FP, Dutta M, Kjeang E. 3D failure analysis of pure mechanical and pure chemical degradation in fuel cell membranes. J Electrochem Soc 2017;164:F1331–41. https://doi.org/10.1149/2.0451713jes.
[21] Mukundan R, Baker AM, Kusoglu A, Beattie P, Knights S, Weber AZ, et al. Membrane accelerated stress test development for polymer electrolyte fuel cell durability validated using field and drive cycle testing. J Electrochem Soc 2018;165:F3085–93. https://doi.org/10.1149/2.0101806jes.
[22] Kusoglu A, Karlsson AM, Santare MH, Cleghorn S, Johnson WB. Mechanical response of fuel cell membranes subjected to a hygro-thermal cycle. J Power Sources 2006;161:987–96. https://doi.org/10.1016/j.jpowsour.2006.05.020.
[23] Kusoglu A, Santare MH, Karlsson AM, Cleghorn S, Johnson WB. Numerical investigation of mechanical durability in polymer electrolyte membrane fuel cells. J Electrochem Soc 2010;157:B705. https://doi.org/10.1149/1.3328496.
[24] Kreitmeier S, Lerch P, Wokaun A, Büchi FN. Local degradation at membrane defects in polymer electrolyte fuel cells. J Electrochem Soc 2013;160:F456–63. https://doi.org/10.1149/1.023306jes.
[25] Zhao J, Li X. A review of polymer electrolyte membrane fuel cell durability for vehicular applications: degradation modes and experimental techniques. Energy Convers Manag 2019;199:112022. https://doi.org/10.1016/j.enconman.2019.112022.
[26] Department of Energy. Append D DOE Solicitation DE-PS36-06GO96017. 2007. 2017. https://www1.eere.energy.gov/hydrogenandfuelcells/fuelcells/pdfs/component_durability_profile.pdf. [Accessed 24 April 2022].
[27] Hashimasa Y, Matsuda Y, Imamura D, Akai M, Sasaki M. Evaluation of MEA durability test protocols. Trans Japan Soc Mech Eng Part B 2011;77:147–59. https://doi.org/10.1299/kikaib.77.147.
[28] Fuel Cell Commercialization Conference of Japan. The membrane electrode assembly (MEA) durability test protocols. 2011. https://fccj.jp/pdf/23_01_kt.pdf. [Accessed 24 April 2022].
[29] Hashimasa Y, Numata T. Comparison of test results on load cycle durability of polymer electrolyte fuel cell cathode catalysts. Int J Hydrogen Energy 2015;40:11543–9. https://doi.org/10.1016/j.ijhydene.2015.04.031.
[30] Ohma A, Shinohara K, Iiyama A, Yoshida T, Daimaru A. Membrane and catalyst performance targets for automotive fuel cells by FCCJ membrane, catalyst, MEA WG. ECS Trans 2011;41:775–84. https://doi.org/10.1149/1.3635611.
[31] Ishikawa Y, Morita T, Nakata K, Yoshida K, Shiozawa M. Behavior of water below the freezing point in PEFCs. J Power Sources 2007;163:708–12. https://doi.org/10.1016/j.jpowsour.2006.08.026.
[32] Wang S, Sun Y, Huang F, Zhang J. Freezing site of supercooled water and failure mechanism of cold start of PEFC. J Electrochem Soc 2019;166:F860–4. https://doi.org/10.1149/2.0041913jes.
[33] Biesdorf J, Stahl P, Siegwart M, Schmidt TJ, Boillat P. When size matters: Active area dependence of PEFC cold start capability. J Electrochem Soc 2015;162:F1231–5. https://doi.org/10.1149/2.0871510jes.
[34] Hwang GS, Kim H, Lujan R, Mukundan R, Spernjak D, Borup RL, et al. Phase-change-related degradation of catalyst layers in proton-exchange- membrane fuel cells. Electrochim Acta 2013;95:29–37. https://doi.org/10.1016/j.electacta.2013.02.017.
[35] Tabe Y, Wakatake N, Ishima Y, Chikahisa T. Ice formation from a supercooled state and water transport through ionomers during PEFC cold startup. J Electrochem Soc 2021;168:064502. https://doi.org/10.1149/1945-7111/ac035b.
[36] Tabe Y, Saito M, Fukui K, Chikahisa T. Cold start characteristics and freezing mechanism dependence on start-up temperature in a polymer electrolyte membrane fuel cell. J Power Sources 2012;208:366–73. https://doi.org/10.1016/j.jpowsour.2012.02.052.
[37] Jinnouchi R, Kudo K, Kodama K, Kitano N, Suzuki T, Minami S, et al. The role of oxygen-permeable ionomer for polymer electrolyte fuel cells. Nat Commun 2021;12:4956. https://doi.org/10.1038/s41467-021-25301-3.
[38] Japan Meteorological Agency. https://www.jma.go.jp/jma/indexe.html.
[39] Drugeot T, Pinton E, Micoud F, Rosini S, Gerard M, Poupin L, et al. Investigation and quantification of irreversible degradations and their sensitivities during the start-up phases of PEMFC by an accelerated emulation approach. 240th ECS Meeting 2021:I01B–1096.
[40] Chen J, Hu J, Waldecker JR. A Comprehensive model for carbon corrosion during fuel cell start-up. J Electrochem Soc 2015;162:F878–89. https://doi.org/10.1149/2.0501508jes.
[41] Takahashi T, Ikeda T, Murata K, Hotaka O, Hasegawa S, Tachikawa Y, Nishihara M, Matsuda J, Kitahara T, Lyth SM, Hayashi A, Sasaki K. Accelerated durability testing of fuel cell stacks for commercial automotive applications: a case study. J Electrochem Soc 2022;169:044523. https://doi.org/10.1149/1945-7111/ac662d.